Available online at www.sciencedirect.com
ScienceDirect
Journal of Fluorine Chemistry 128 (2007) 296–310
JOURNAL OF FLUORINE CHEMISTRY
www.elsevier.com/locate/fluor

Review

Electrochemical synthesis and application of NF_3

Akimasa Tasaka *

Doshisha University, Faculty of Engineering, Department of Molecular Science and Technology, 1-3 Miyako-dani, Tadara, Kyotanabe, Kyoto 610-0321, Japan

Received 30 August 2006; received in revised form 27 October 2006; accepted 30 October 2006
Available online 18 November 2006

Abstract

Electrolytic production of nitrogen trifluoride (NF_3) was reviewed. Electrolytic production of NF_3 using a nickel anode is more useful method from view points of the yield and purity of NF_3, especially, free from carbon tetrafluoride (CF_4), but has a few problems to be solved. At present, electrolysis of a molten NH_4F–KF–HF system using a carbon anode is developing, because no anode consumption and no storage of nickel sludge in the melt take place.

Reaction of NF_3 with phosphorus sulfide, preparation of functionally gradient fluorocarbon films and carbonaceous thin films by plasma technique using NF_3, and reactive ion etching of Si, SiO_2, and SiC using NF_3 plasma were reported for the purpose of development on application of NF_3.

Keywords: Nitrogen trifluoride; Electrochemical fluorination; Plasma etching; Functional thin film; Silicon carbide

Contents

1. Introduction

Nitrogen trifluoride (NF_3), which has physicochemical properties as shown in Table 1, is a stable gas at room temperature and has a strong oxidation power at higher temperature [1–3]. At up to about 200 °C, its reactivity is comparable to oxygen. Over 200 °C, the dissociation of NF_3 into NF_2 and free fluorine radical becomes significant. The free fluorine radical reacts with most organic compounds and certain metals, liberating heat and causing further dissociation of NF_3. Over 400 °C, the reactivity of NF_3 becomes more like that of fluorine. The thermal dissociation of NF_3 has been

* Tel.: +81 774 65 6592; fax: 81 774 65 6841.
E-mail address: atasaka@mail.doshisha.ac.jp.

0022-1139/$ – see front matter © 2006 Elsevier B.V. All rights reserved.
doi:10.1016/j.jfluchem.2006.11.007

Table 1
Physicochemical properties of nitrogen trifluoride (NF_3)

Properties	Value
Melting point (°C)	−206.8
Boiling point (°C)	−129.1
Liquid density (g/mL)	1.533
Heat of vaporization (kJ/mol)	11.59
Triple point (°C/0.263 Pa)	−206.8
Heat of fusion (J/mol)	398
Solid transition point (°C)	−216.5
Heat of transition (kJ/mol)	1.513
Critical temperature (°C)	−39.25
Critical pressure (kPa)	4530
Critical volume (cm^3)	123.8
Heat of formation (kJ/mol)	−131.5
Heat capacity (J/(mol K) at 25 °C)	53.59
Water solubility (mol NF_3/mol H_2O)	1.4×10^{-5}
Dipole moment (Debye)	0.234
Bonding energy	238.91
NF_2–F (kJ/mol)	
NF–F (kJ/mol)	297.06
N–F (kJ/mol)	297.06
Vapor pressure equation (kPa)	$\log P = 5.90445 - 501.913/(T - 15.37)$

studied by a number of researchers [4–7] and was found to peak in the temperature range of 800–1200 °C. Therefore, it has been already used as an oxidizing agent for rocket fuels and a stable fluorinating agent [8–15]. It may be also used as a welding agent for metals and a gas-filler in order to increase the life and the brightness of lamps [16].

After early 1980's, electronics industry has been dramatically growing up. A few researches have been attempted to develop the use of NF_3 as a laser gas [17–19], an etching gas (etchant) for a dry etching process [20–23] and a cleaning gas for apparatus used in the CVD technique [24]. The advantage of using NF_3 as an etchant over traditional carbon based etchants such as carbon tetrafluoride (CF_4) and hexafluoroethane (C_2F_6) includes high etching rate, high selectivity for nitride-over-oxide etching and single crystal silicon over thermally grown silicon oxide, and the production of only volatile reaction products, resulting in an etching without carbon based polymer or fluoride residues. Enhanced plasma or thermal cleaning of chemical vapor deposition (CVD) chambers is also a use of NF_3. Residual coating such as silicon are deposited on the internal surfaces of CVD chambers during deposition processes. A plasma using NF_3 can remove these deposits as volatile fluoride like SiF_4 at the process temperature, eliminating the need to remove the internal CVD chamber components to be cleaned by acid tank immersion. At present, large amounts of NF_3 is consumed as a dry etchant and a cleaning gas for the CVD chamber by the electronic industry in Japan.

In mid-1990's, the commercial production of NF_3 was started in Japan. Then, some processes for the production of NF_3 have been proposed. A few of them are now industrialized and the electrochemical process is better than the chemical process in the view points of the yield and purity of NF_3, especially, free from carbon tetrafluoride (CF_4). High pure NF_3 (99.99%) free from CF_4 can be obtained by the electrolysis of $NH_4F{\cdot}2HF$ with a nickel anode followed by purification to meet demand. In a divided cell of 3000–4000 A having nickel anodes, extensive dilution of the gas streams with N_2 was used to prevent explosive reactions between NF_3 and H_2 [25]. Nickel, however, is corroded to some extent, and corresponds to current loss of 3–5%. Deposition of NH_4NiF_3 on the cell bottom is also another problem to be solved.

Electrolysis of a molten NH_4F–KF–HF system using carbon anode may be available for production of NF_3. This process is free from corrosion and passivation of the anode. However, it has in drawbacks such as the occurrence of the anode effect, breakdown of the anode, and contamination of NF_3 with a small amount of CF_4. Recently, a new isotropic carbon FE-5 and LiF-impregnated carbon (LFIC) anodes were developed to suppress the anode effect and a gradual increase in electrolytic voltage in production of fluorine (F_2) [26]. Using pristine carbon FE-5, fluorine gas with a trace amount of CF_4 can be produced. It has been reported that fluorine-graphite intercalation compounds (GICs) with semi-covalent C–F bonds, $(C_xF)_n$, which have a higher surface energy and a high electric conductivity, are easily formed on the LFIC anode, so that it may have a better wettability by the melt than the pristine carbon FE-5 anode [26–28]. The pristine carbon FE-5 and the LFIC anodes can produce NF_3 free from or with a trace amount of CF_4 in a molten NH_4F–KF–HF system, and hence the LFIC anode can be used for a long period without the anode effect. The current efficiency for NF_3 formation on a carbon FE-5 is ca. 60%, which is almost equal to that on the nickel anode [29].

In this paper, two electrolytic processes of NF_3 production using a nickel and a carbon anodes and a few applications of NF_3, i.e., preparation of phosphasen by reaction of NF_3 with phosphorus sulfide, production of fluorinated film and the sp^2-like carbon film from mixture gas of hydrocarbon and NF_3 using plasma polymerization technique and reactive ion etching of Si, SiO_2, and SiC using pure NF_3 and NF_3/O_2 mixture gas plasma, are described in detail.

2. Electrolytic processes for NF_3 production

2.1. Electrolysis of $NH_4F{\cdot}2HF$ melt with a nickel anode

This method is employed at present for electrolytic production of NF_3 in an industrial scale in Japan. On the bases of papers reported by Glemser et al. [30] and Massonne [31], the author studied the electrolysis of the $NH_4F{\cdot}2HF$ melt with the nickel anode in order to develop the electrolytic process as one for manufacture of NF_3. Mitsui Chemicals Inc. developed this process in the facility site at Shimonoseki under advising of the author and with full supports of the author.

2.1.1. Electrolytic cell

The metals can be classified in four classes on the bases of the characteristics of the oxidized layer formed on the metallic anode in a well dehydrated melt of $NH_4F{\cdot}2HF$ as shown in Table 2. Table 2 indicated that nickel and carbon are available

Table 2
Classification of various metals and alloys on the base of their anodic behaviors

Class	I	II	III	IV
Formation of film	None	Passive film		
Characteristic of film	——	Insulating	Conductive (Noble metal)	Conductive
Anode material	Al Mo Nb Pb Sn Ta Ti W [Fe]	Ag Cu Co Fe Zn	Au Pd Pt	Ni Monel (Ni 66.5, Cu 33.5) [C]
	Nickel- based Alloy (Composition; wt %) Hastelloy C-4 (Ni 68, Cr 16, Mo 16, Low C, Low Si) Hastelloy C-22 (Ni 58, Fe 4, Cr 22, W 3, Mo 13, Low C, Low Si) MA 45C (Ni 68, Cr 16, Mo 16, Low C) MA 55C (Ni 50, Cr 30, Mo 20) MA 600C (Ni 78, Fe 7, Cr 15) MA 625C (Ni 63.3, Fe 2.5, Cr 21.5, Nb+Ta=3.7) HA-214 (Ni 79.5, Al 4.5, Cr 16)			

as the anode for electrochemical fluorination of molten fluorides containing HF.

A cylindrical nickel cell of 1.5 dm^3 in volume as shown in Fig. 1 was employed in the experiments for developing the electrolytic production of NF_3. The nickel sheets of 24 and 66 cm^2 in surface area were used as the anode. The Ni rod of 1.0 cm^2 in surface area with pre-treatment of anodic oxidation in a well dehydrated melt of $NH_4F{\cdot}2HF$ or thermal fluorination of NF_3 at 300 °C was used as the reference electrode. The measured potential was 0.076 V against the potential for hydrogen evolution on a Pt electrode at 100 °C and hence it is considered to function as the Ni/NiO_xF_y electrode [32]. However, it is denoted as the Ni/NiF_2 reference electrode, conventionally. Although the electrode potential was measured against the static potential of the Ni/NiF_2 reference electrode, it was calibrated to a new scale referred to the potential for hydrogen evolution, and was presented in volts versus H_2. A metallic skirt was provided between the anode and the cathode to separate the anode gas from hydrogen generated at the cathode so that explosion and the loss of NF_3 are prevented. The cell bottom was covered with the PTFE sheet to avoid hydrogen evolution. The electrolyte was charged in the cell placed in air, and hence the water content seemed to be more than 0.02% at start of electrolysis.

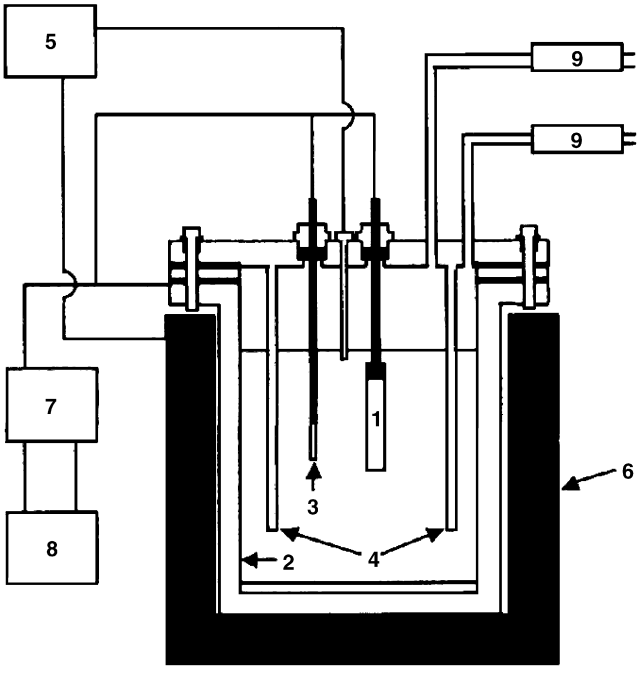

Fig. 1. Cylindrical metallic cell for electrolytic production of NF_3. (1) Anode (Ni sheet, 24 or 66 cm^2), (2) cathode (inside wall of metallic cell), (3) reference electrode (Ni/NiF_2, F^-, 76 mV ± 5 mV, (4) skirt, (5) thermometer, (6) heater, (7) potentio-galvanostat, (8) recorder, and (9) HF absorber (NaF pellets).

$NH_4F{\cdot}2HF$ was prepared with extra pure HF (99.99%) and NH_4F (99.9%) in a dry box. Electrolysis was conducted with the electrolytic cells at 100 or 120 °C. Although the water content was high before start-up, it might be decreased by electrolysis to less than 0.02 wt% within 80 h [33]. The anode gas was treated with NaF to eliminate HF. Its sample gas was fractionated by means of gas chromatography (column packing: Porapack R and molecular sieve 5A; carrier gas: He) and analyzed by infrared spectroscopy and/or mass spectroscopy to identify the constituents having the respective peaks on the chromatogram.

2.1.2. Electrolysis

Fig. 2 shows an example of the time variation of the gas composition. Water in the melt was electrolyzed in preference

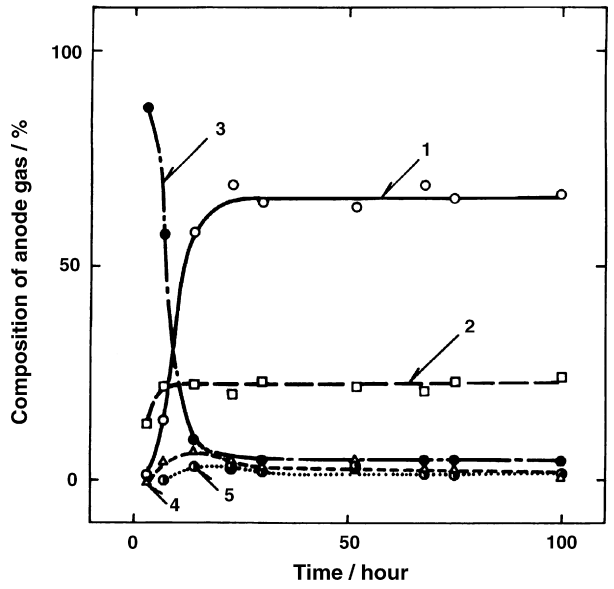

Fig. 2. Time variation of the gas composition by electrolysis of $NH_4F{\cdot}2HF$ melt at 25 mA/cm^2 and 120 °C in the nickel cell. Condition: nickel anode, surface area = 66 cm^2. 1: (○); NF_3, 2: (□); N_2, 3: (●); O_2, 4: (△); N_2O, 5: (◑); N_2F_2.

to the fluorination of NH_4^+ for some 30 h after start-up. NF_3 was the main product, followed by N_2 with a small amount of O_2, N_2O, N_2F_2, and N_2F_4. Under the conditions of interest, NH_4^+ and NH_3 are in equilibrium, as shown in Eqs. (1) and (2)

$$NH_4F + nHF \rightleftarrows NH_4^+ + F(HF)_n^- \quad (1)$$

$$NH_4^+ + mHF \rightleftarrows NH_3 + H(HF)_m^+ \quad (2)$$

where $F(HF)_n^-$ and $H(HF)_m^+$ are the solvated ions of F^- and H^+, respectively, and are now written as F^- and H^+ for simplicity. The amount of NH_3 in the melt is generally considered negligible. Nitrogen trifluoride and nitrogen are evolved at the anodes by reactions (3) to (4′) [27,34–36].

$$NH_4^+ + 7F^- \rightarrow NF_3 + 4HF + 6e \quad (3)$$

$$2NH_4^+ + 8F^- \rightarrow N_2 + 8HF + 6e \quad (4)$$

$$2NH_3 \rightarrow N_2 + 6H^+ + 6e \quad (4')$$

where reaction (4′) is the direct discharge of NH_3 adsorbed on the anode. However, the side reactions (5)–(8′) may also proceed in parallel to form minor products, e.g. N_2F_2, N_2F_4, N_2O, and O_2,

$$2NH_4^+ + 10F^- \rightarrow N_2F_2 + 8HF + 8e \quad (5)$$

$$2NH_4^+ + 12F^- \rightarrow N_2F_4 + 8HF + 10e \quad (6)$$

$$2NH_4^+ + H_2O + 10F^- \rightarrow N_2O + 10HF + 8e \quad (7)$$

$$2H_2O + 4F^- \rightarrow O_2 + 4HF + 4e \quad (8)$$

$$2H_2O \rightarrow O_2 + 4H^+ + 4e \quad (8')$$

where reaction (8′) is the direct discharge of water adsorbed on the anode. Since we have the percentage composition of these gases (Fig. 2) and the total volume produced, it is easy to calculate the current efficiencies for the constituents in the anode gas and for the overall anode gas. Table 3 shows the current efficiencies for the constituents in the anode gas and the overall efficiencies with the current inefficiency caused

Table 3
Current efficiencies of each constituent and overall in anode gas and cathode gas and current loss caused by nickel dissolution in electrolysis of various melts at 25 mA/cm^2 and 120 °C for 100 h

Melts	Current efficiencies (%)								Current loss caused by Ni dissolution (%)
	Anode gas							Cathode gas	
	NF_3	N_2	O_2	N_2F_4	N_2F_2	N_2O	Overall	H_2	
$NH_4F{\cdot}2HF$[a]	49.2	20.1	9.26	4.83	1.47	7.18	92.0	92.0	2.51
$NH_4F{\cdot}2HF$[b]	45.2	23.1	4.22	4.16	1.32	5.21	83.2	87.2	2.45
$NH_4F{\cdot}2HF$ + 0.1 mol% LiF[b]	53.0	19.9	4.46	5.56	0.77	3.51	87.2	88.1	1.47
$NH_4F{\cdot}2HF$ + 0.3 mol% LiF[a]	68.3	12.6	3.41	4.25	0.54	4.56	93.7	94.6	1.37
$NR_4F{\cdot}2HF$ + 0.3 mol% LiF[b]	53.3	24.1	6.15	3.22	0.67	1.15	88.6	88.7	1.37
$NH_4F{\cdot}2HF$ + 0.9 mol% LiF[b]	54.8	18.4	8.70	2.98	1.14	1.24	87.3	87.7	1.36
$NH_4F{\cdot}2HF$ + 6.7 mol% CsF[a]	59.0	19.1	0.61	5.75	1.15	7.75	93.4	95.3	2.85
$CsF{\cdot}3NH_4F{\cdot}8HF$ (8.3 mol%)[b]	49.8	21.9	4.43	7.26	1.66	3.38	88.4	89.1	1.59
$CsF{\cdot}2NH_4F{\cdot}6HF$ (11.1 mol%)[b]	55.5	22.1	4.31	3.13	0.65	3.33	89.0	89.7	1.46
$CsF{\cdot}NH_4F{\cdot}4HF$ (16.7 mol%)[b]	36.1	33.7	8.52	3.61	0.80	2.69	85.4	90.1	1.39
$NH_4F{\cdot}2HF$ + 0.3 mol% NaF[a]	57.9	11.1	6.79	6.57	0.92	8.86	92.1	92.9	2.01
$NH_4F{\cdot}2HF$ + 6.7 mol% NaF[a]	56.9	25.3	2.11	4.24	0.85	2.72	92.1	94.0	3.14
$NH_4F{\cdot}2HF$ + 0.3 mol% KF[a]	52.1	18.0	7.15	2.99	1.51	6.79	88.5	89.5	2.79
$NH_4F{\cdot}2HF$ + 6.7 mol% KF[a]	48.0	30.7	1.21	3.55	0.49	5.84	89.8	92.6	3.40
$KF{\cdot}3NH_4F{\cdot}8HF$ (8.3 mol%)[b]	39.8	35.9	3.91	0.66	0.21	2.73	83.2	83.2	3.81
$KF{\cdot}2NH_4F{\cdot}6HF$ (11.1 mol%)[b]	40.4	35.2	2.11	0.49	0.14	4.50	82.8	81.3	4.12
$KF{\cdot}NH_4F{\cdot}4HF$ (16.7 mol%)[b]	37.8	32.1	6.01	0.42	0.67	3.14	80.1	80.2	5.16

Nickel anode = 24 cm^2.
[a] Hours on line = 100.
[b] Hours on line = 80.

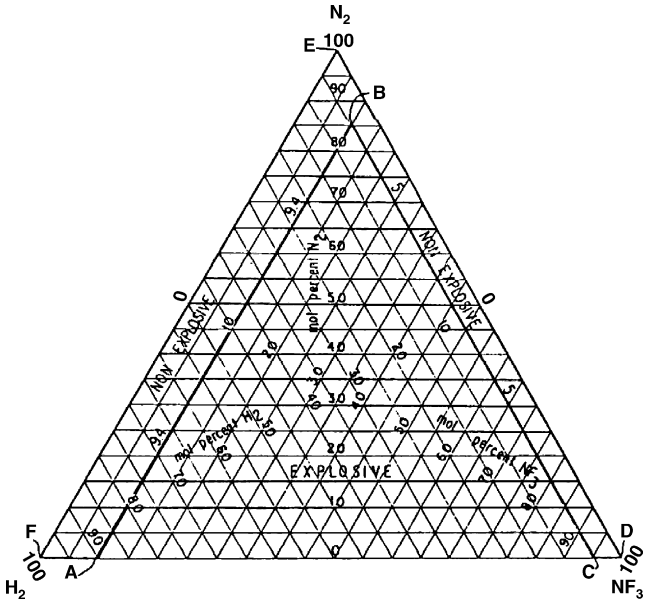

Fig. 3. Limited composition of explosion in the mixture of H_2–NF_3–N_2 system [34].

by the dissolution of the nickel anode. The current loss caused by nickel dissolution was calculated from the weight loss with the assumption of two-electron transfer for the reaction (9)

$$Ni \rightarrow Ni^{2+} + 2e \quad (9)$$

Table 3 indicated that addition of LiF to the melt increased the current efficiency for NF_3 formation and decreased the anodic consumption.

When the skirt made of monel was used, explosion often took place. This may be suggested that anode gas was mixed with hydrogen in the anode compartment. Fig. 3 shows the limited composition of explosion in the mixture of H_2–NF_3–N_2 system [25]. This may be caused by bipolarization of metallic skirt. In this case, the inside of skirt acted as the cathode to evolve hydrogen in the anode compartment. Table 4 shows the weight loss of metallic anode in the molten $NH_4F{\cdot}KF{\cdot}4HF$ during potentiostatic electrolysis. The cathode potential was ca. 1 V versus H_2, so that its outside made of monel might be able to act as the anode to be dissolved in the cathode compartment. The extensive dilution of the gas streams with N_2 and the coverage of the monel skirt with PTFE film was used to prevent explosive reactions between NF_3 and H_2.

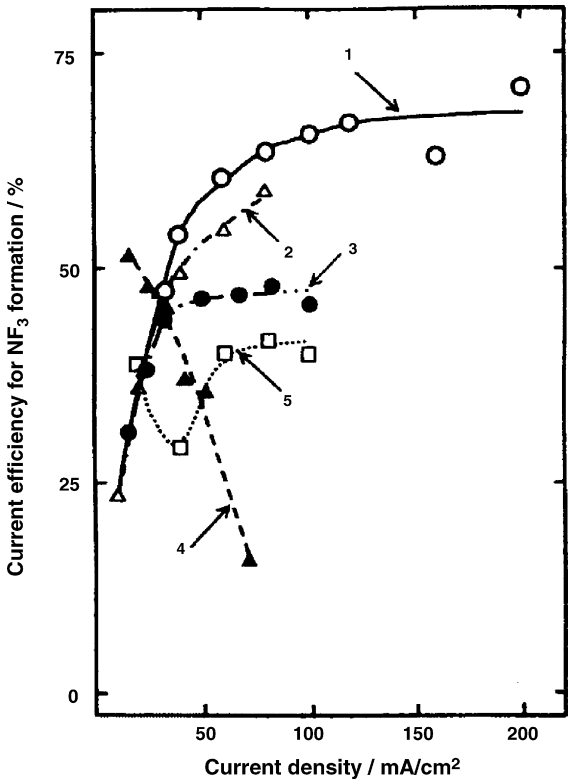

Fig. 4. Relation between the current efficiency for NF_3 formation and the current density. 1: (○) Ni anode, $NH_4F{\cdot}1.7HF$, 100 °C, 2: (△) Ni anode, $KF{\cdot}NH_4F{\cdot}4HF$, 100 °C, 3: (●) LiF/C anode, $NH_4F{\cdot}1.7HF$, 100 °C, 4: (▲) LiF/C anode, $KF{\cdot}NH_4F{\cdot}4HF$, 100 °C, and 5: (□) Ni anode, $CsF{\cdot}NH_4F{\cdot}4HF$, 80 °C.

Fig. 4 shows the current efficiency for NF_3 formation as a function of the current density under various conditions [27,34,35]. The open circles and closed circles represent the experimental results with the Ni anode and the LiF-impregnated carbon (LiF/C) anode, respectively. Apparently, the overpotential of the LiF/C anode is relatively low in an NH_4F–HF melt, and results in a low rate of disintegration of carbon anode. Therefore, its material is applicable to our experiment. The current efficiencies for NF_3 formation on the Ni and the LiF/C anodes in the $NH_4F{\cdot}1.7HF$ melt increased with the current density, and they reached constant values at 120 and 50 mA/cm^2, respectively. The constant current efficiency on the Ni anode (ca. 68%) was large compared with that on the LiF/C anode (ca. 47%). In the presence of K^+ ion, the current efficiency for NF_3 formation on the Ni anode decreased over the entire range of current density studied. On

Table 4
Weight loss of metallic anode in the molten $NH_4F{\cdot}KF{\cdot}4HF$ during potentiostatic electrolysis.

Anode	Potential (V vs. Pt)	C.D. (mA cm^{-2})	D.E. (h)	Q.E. (C)	n	Weight loss of anode (g)	Rate (g hr^{-1} cm^{-2}	Q_n/Q_t (%)
Nickel	1.0	0.12–0.22	24	32.62	2	0.0093	1.94×10^{-4}	94
Iron	1.0	0.025	22	4.30	2	0.0010	2.27×10^{-5}	80
Monel	1.0	0.065–0.27	25	40.18	2(Ni), 2(Cu)	0.0106	2.12×10^{-4}	87, 80
Copper	1.0	0.83–1.7	24	251.77	2	0.0834	1.74×10^{-3}	101

C.D., current density; D.E., duration of electrolysis; Q.E., quantity of electricity; n, valence; Q_n/Q_t, ratio of quantity of electricity dissipated by anodic dissolution of electrode to total quantity of electricity, *Conditions*: area of electrode; 2 cm^2, temperature; 120 °C.

the other hand, the NF_3 current efficiency on the LiF/C anode in $KF{\cdot}NH_4F{\cdot}4HF$ decreased with the current density, and reached only 16% at 70 mA/cm^2. Also, the NF_3 current efficiency varied with the concentration of alkali metal fluoride and the operating temperature.

Fig. 5 shows the formation mechanism of NF_3 from ammonia (NH_3) and/or ammonium ion (NH_4^+) proposed by Tasaka et al. [35–37]. At first, fluoride ion can be discharged on the carbon anode polarized at potentials higher than ca. 3 V to form atomic fluorine, i.e., fluorine radical. The fluorine radicals produced fluorinate the starting material of NH_3 and/or NH_4^+ to form NF_3. In the case of lack of fluorine radical against the amount of NH_3 and/or NH_4^+ at the anode, byproducts such as N_2, N_2F_2, and N_2F_4 are formed. In the case of excess of fluorine radical on the anode surface, fluorine radicals on the anode surface are combined to form F_2 molecules, and diffuse to the bulk electrolyte. These species react NH_4^+ to form mainly N_2. The current efficiency for NF_3 formation on the carbon anode is low, since side reactions such as N_2 formation are relatively fast, especially at current densities higher than 30 mA/cm^2. Fluoride ions can discharge also on the nickel anode, and fluorine radicals combine with nickel to form nickel fluoride on the anode. This layer is composed of NiF_x and/or NiF_xO_y, in which the valance of nickel ions is high, 3 or 4 rather than 2. These species, i.e., highly oxidized nickel fluorides such as NiF_3, Ni_2F_5, and Li_2NiF_6 on the anode and the complex ions such as NiF_6^{3-} and NiF_6^{2-} in the melt are catalytically active and fluorinate NH_3 and/or NH_4^+ to NF_3 as a reaction mediator [27,37,38]. In other words, the multi-valance compounds on the nickel anode and in the melt near the anode are indispensable for the electrochemical fluorination of NH_3 on the anode and/or NH_4^+ in the melt, and the mechanism differs from that on the carbon anode.

The highly oxidized nickel fluorides such as NiF_3, Ni_2F_5, and Li_2NiF_6 on the anode and the complex ions such as NiF_6^{3-} and NiF_6^{2-} in the melt fluorinate NH_3 and/or NH_4^+ through their respective reactions. The products such as NiF_2 and NiF_3^- at the nickel anode oxidized further to highly oxidized nickel fluorides and complex ions having trivalent and tetravalent states. These species would play an important role in the electrochemical fluorination process at the nickel anode in a molten NH_4F–HF system and other systems.

The electrolytic conditions in manufacturing NF_3 in the industry scale are the molar ratio range of HF/NH_4F between 1.8 and ca. 2 in the melt containing LiF, current density range of 25–100 mA/cm^2, and temperature range of 100–120 °C. The current efficiency for NF_3 formation is ca. 65–70% and current loss caused by anodic dissolution is ca. 1%. The raw NF_3 produced is refined and NF_3 with high purity of 99.99–99.999% free from CF_4 can be obtained through refinement of the raw NF_3 produced by electrolysis.

The characteristics of the process with a nickel anode are as follows:

(1) NF_3 with high purity free from CF_4 can be obtained.
(2) The yield in this process is higher than that in the chemical process.
(3) No anode effect takes place during electrolysis.
(4) The weight loss caused by Ni anodic dissolution is lower than 3% of electricity during electrolysis.
(5) The sludge of NH_4NiF_3 is stored in the electrolytic cell.
(6) Vapor pressures of NH_3 and HF on the molten NH_4F–HF system is relatively high, so that the melt losses and the outlet line of gas is packed with NH_4F condensed from NH_3 and HF.
(7) Removal of the condensed NH_4F from the inside of the gas line is needed.

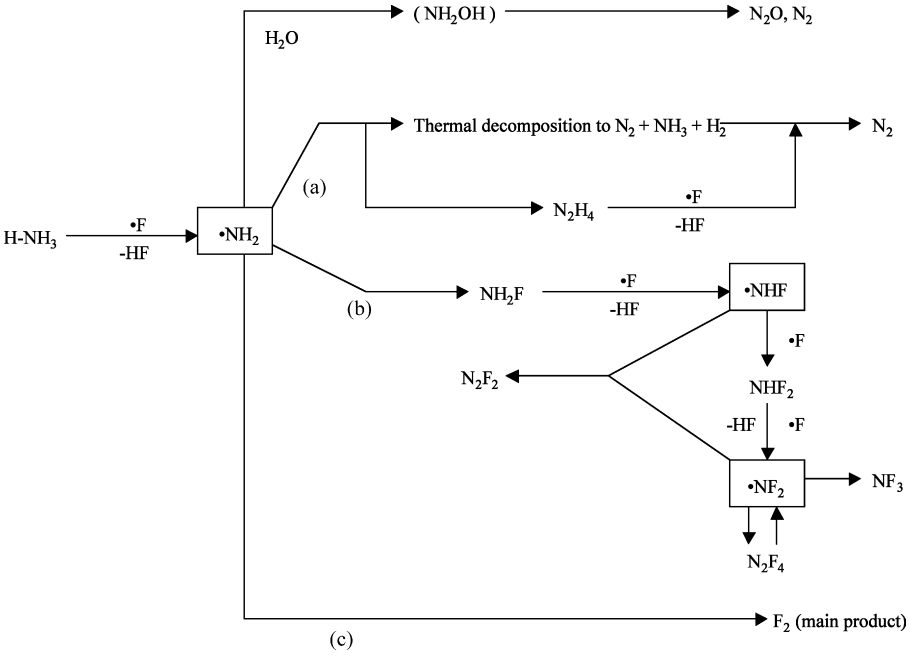

Fig. 5. Mechanism on NF_3 formation from ammonia (NH_3) and/or ammonium ion (NH_4^+) in electrolysis of the $NH_4F{\cdot}2HF$ or NH_4F–KF–HF melts.

2.2. Electrolysis of the molten NH_4F–KF–HF system with a carbon anode

The molten NH_4F–KF–HF system has a higher surface energy and a higher electrolytic conductivity. Also, it has a relatively low vapor pressure of HF and a higher viscosity so as to suppress the penetration of HF into the pore of carbon anode and the breakdown of carbon anode. Hence, the carbon anode can be used as the anode for electrolytic production of NF_3.

2.2.1. Electrolysis

The composition of anode gas is dependent upon the current density, the concentration of starting material such as NH_4F and amine, and the anode potential [27,34–36]. NH_4F is the best starting material for production of NF_3 with a lower concentration of CF_4. When a melt contains a certain concentration of water, N_2, N_2O, O_3, and O_2 were formed at the carbon anode and NF_3 was produced after electrolysis for more than a week. Hence, the molten NH_4F–KF–HF system containing a trace of water should be used as the electrolyte in order to obtain NF_3 by electrolysis for shorter duration.

The electrolytic conditions for electrolytic production of NF_3 from the molten NH_4F–KF–HF system using a carbon anode (FE-5) are the NH_4F concentration of 15–25 mol% in the melt containing LiF, current density range of 10–20 mA/cm^2, temperature range of 120–150 °C, and the cell voltage of ca. 6–7 V. The current efficiency for NF_3 formation is ca. 60%.

The characteristics of the process with a carbon (FE-5) anode are as follows:

(1) The molten NH_4F–KF–HF system has a higher electrolytic conductivity.
(2) The molten NH_4F–KF–HF system has a relatively low vapor pressure of HF on the melt.
(3) Existence of KF in the melt suppresses penetration of HF into the pore of a carbon anode.
(4) Current efficiency for NF_3 formation is high.
(5) Carbon steel can be used as the structural material for electrolytic cell.
(6) Anode effect takes place during electrolysis.
(7) Carbon anode sometimes breaks down during electrolysis.
(8) NF_3 is contaminated with CF_4, whose concentration is lower than 1%.

3. Application of NF_3

3.1. Preparation of fluorophosphasen by reaction of NF_3 with phosphorus sulfide [15]

NF_3 can be used as a stable fluorinating material. Many reactions using NF_3 as a fluorinating agent were reported by Glemser et al. [11–14]. A trace of fluorophosphasen was formed by reaction of NF_3 with phosphorus, whereas cyclic fluorophosphasen of $(NPF_2)_n$ was formed with the high yield by reaction of NF_3 with phosphorus sulfide. Table 5 shows the results from reaction of NF_3 with phosphorus sulfide such as P_4S_3 and P_4S_{10}. In a nickel trap at 180–215 °C $(NPF_2)_n$ (n = 3–9) is formed in good yield of 60% together with PF_3 and PF_5. In this case, no nitrogen was formed during reaction of NF_3 with P_4S_3. This means that all nitrogen atoms in NF_3 may be introduced in the product $(NPF_2)_n$. At higher temperatures also SPF_3 with SF_4 and SF_6 are produced in considerable amounts. This is a first reaction by which fluorophosphasen can be produced in only one step and nitrogen in NF_3 molecule is introduced in a product.

3.2. Preparation of functionally gradient fluorocarbon polymer films by plasma polymerization of NF_3 and propylene [39]

Plasma polymerization is an attractive technology to prepare thin polymer films and has recently applied to the preparation of fluorinated thin films with a highly cross-linked structure. Since plasma-polymerized fluorocarbon films are uniform and pinhole-free as well as chemically and thermally inert, they are promising as protective films on solid materials against corrosive environments.

Thin fluorocarbon polymer films were prepared by plasma polymerization using nitrogen trifluoride (NF_3) and propylene as starting materials. To improve their adhesiveness to substrates, a novel functionally gradient film in which the content of fluorine decreased continuously from the surface to the interior was prepared by changing source gas composition during deposition.

Fluorocarbon polymer films have many excellent properties such as chemical and thermal stability and high repellence to water, etc., and thus are promising as protective films on solid materials against corrosive environments. However, highly

Table 5
Reaction of NF_3 with P, P_4S_3 and P_4S_{10}

Reaction partner	Reactant	Flow rate (l/h)	Reaction temperature (°C)	Reaction time (h)	Product	Yield (%)	Other products
P	NF_3	–	400–460	–	$(NPF_2)_3$	Trace	
P_4S_3	NF_3	0.4	180–215	7.7	$(NPF_2)_n$; n = 3–9	60	PF_3, PF_5, S
	NF_3	0.6	220–270	8.8	$(NPF_2)_n$; n = 3–9	23	SPF_3, SF_6(+SF_4), PF_3, N_2
	NF_3	0.5	328–360	15.5	$(NPF_2)_n$; n = 3–9	10	SPF_3, SF_6(+SF_4), PF_3, N_2
	NF_3	0.9	340–360	4.4	$(NPF_2)_n$; n = 3–9	23	SPF_3, SF_6(+SF_4), PF_3, PF_5, N_2
P_4S_{10}	NF_3	1.8	345–365	3.0	$(NPF_2)_n$; n = 3–9	20	SPF_3, SF_6(+SF_4), PF_5, N_2
	NF_3	2.6	400–440	1.9	$(NPF_2)_n$; n = 3–9	15	SPF_3, SF_6(+SF_4), N_2

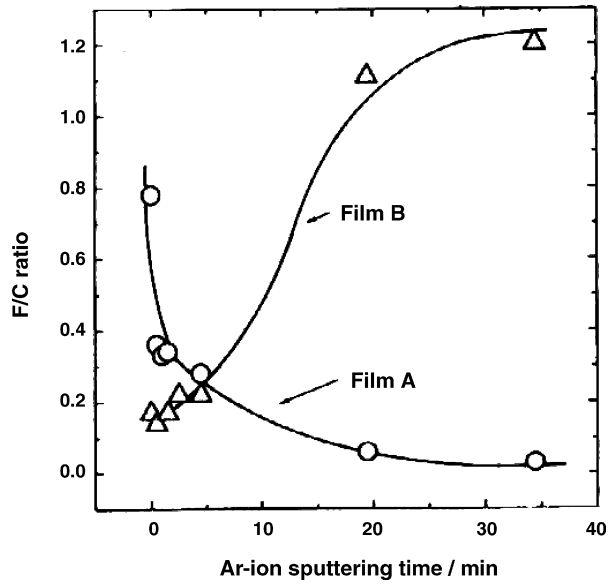

Fig. 6. Depth profiles of F/C ratio of film A (○) and film B (△) measured by XPS. The abscissa denotes the sputtering time by argon ion beam.

fluorinated films show poor adhesion to inorganic solids. To overcome the drawback, we prepared fluorocarbon polymer films with gradual variations of fluorine content from the surface to the interior by changing flow rates of NF_3 (U_{NF}) during polymerization. The flow rate of propylene (U_{CH}) was fixed at 10 cm^3 (STP)/min and total pressure was maintained at 30 Pa. Film A was prepared from the surface to the interior by decreasing the flow rate of NF_3 and film B by increasing the flow rate of NF_3. The surfaces of both films were flat, uniform and free from pinholes. The depth profile of the F/C ratio of each film was analyzed by XPS using argon-ion beam sputtering, and is shown in Fig. 6. For film A, the F/C ratio decreased with increasing sputtering time. This decrease in F/C ratio cannot be attributed to a difference in sputtering ratio between carbon and fluorine atoms because such a decrease in F/C ratio was not observed in the case of a commercially available polytetrafluoroethylene film. Hence, the observed decrease in F/C ratio indicates that the fluorine content decreased continuously from the surface to the interior. On the other hand, the F/C ratio increased from the surface to interior for film B. These results clearly show that the chemical composition of the plasma film can be varied from the surface to the interior by changing U_{NF} during polymerization. Fig. 7 shows SEM photographs of film A. The thickness of film A was about 7 μm. The surface of film A was smooth and pinhole-free (Fig. 7(a)), and the film adhered tightly to the substrate (Fig. 7(b)). The water contact angle of the gradient film A for water drop was 110.0° and was comparable to that polytetrafluoroethylene (108–112°). On the other hand, the contact angle of the hydrocarbon film prepared without NF_3 was 99.0°. These results show that the only local fluorination in the vicinity of the surface improved the repellence to water. Consequently, this gradient plasma polymerization film, film A, is a promising material as a protective film on solid materials against corrosive environments.

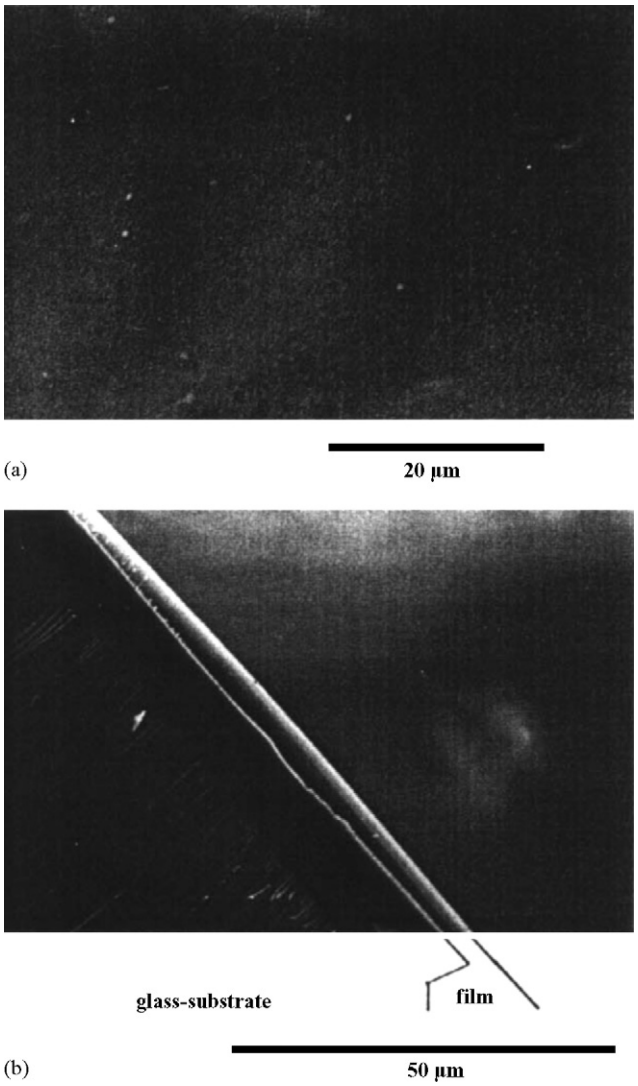

Fig. 7. SEM photographs of surface (a) and cross-section of film A (b).

3.3. Preparation of carbonaceous thin film by C_2H_4/NF_3 glow discharge plasma [40]

Plasma assisted chemical vapor deposition (PCVD) has been used for the preparation of inorganic materials, mainly because the chemical reactions are accelerated in plasma at low temperature and the resulting films prepared by PCVD are dense and pinhole-free. Carbonaceous thin films were prepared from ethylene, argon and nitrogen trifluoride (NF_3) by plasma assisted chemical vapor deposition (PCVD). The carbon thin films were characterized by scanning electron microscope (SEM). Their electrochemical properties were studied by cyclic voltammetry and charge and discharge measurements.

From SEM image of carbon thin films was flat and pinhole-free. XPS spectra indicate that nitrogen and fluorine atoms are not contained in carbon thin films. Fig. 8 shows the Raman spectra of carbon thin films. Mainly two peaks around 1360 and 1580 cm^{-1} were observed. These peaks have been known as Raman active A_{1g} (due to finite crystal size) and E_{2g} (due to infinite crystal size) mode frequencies, respectively [41]. The

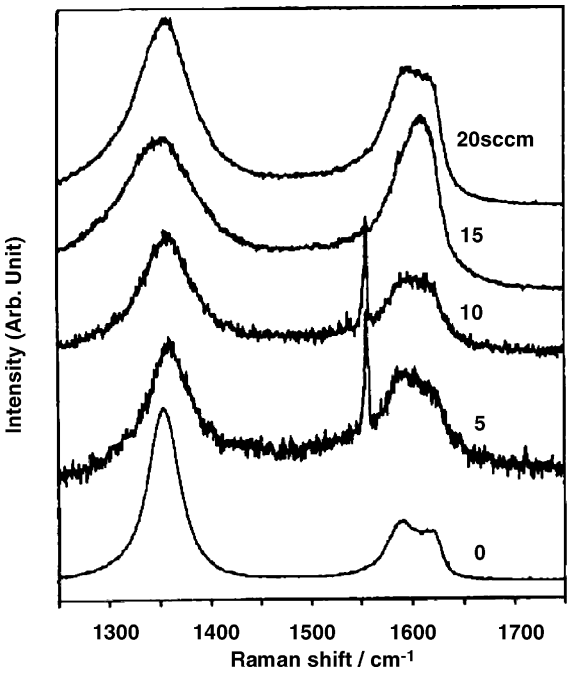

Fig. 8. Raman spectra of carbon thin films prepared by PCVD at various flow rate of NF_3. Applied RF power = 50 W. Numbers in the figure represent the flow rate of NF_3.

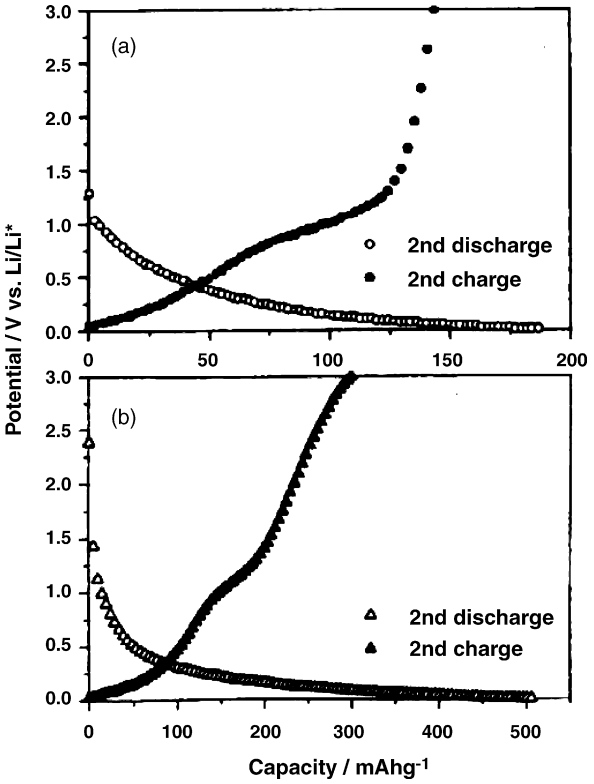

Fig. 9. Charge and discharge characteristics of carbon thin films prepared at various flow rate of NF_3 of the second charge and discharge cycle in 1 mol/dm^3 $LiClO_4$/EC + DEC (1:1). Applied RF power = 50 W. (a) Flow rate of NF_3 = 15 sccm, (b) flow rate of NF_3 = 20 sccm.

peak around 1620 cm^{-1} is also derived from imperfection of graphite crystal [42]. The intensity ratio of peak around 1360 cm^{-1} to that around 1580 cm^{-1}, (I_{1360}/I_{1580}), correlates with the degree of crystallinity [43]. Crystallinity of the films is affected by the NF_3 flow rate from Raman spectra, as shown in Fig. 8. Hence, the samples prepared by the NF_3 flow rate of 15 and 20 sccm are similar to that of graphitizable carbon [44].

The difference of the NF_3 flow rates also affected the results of cyclic voltammetry and charge and discharge measurements. Fig. 9 shows charge and discharge characteristics of carbon thin films prepared at various flow rate of NF_3 of the second charge and discharge cycle in 1 mol/dm^3 $LiClO_4$/EC + DEC (1:1). Upper figure, labeled (a), is the results of specimen A prepared at the NF_3 flow rate of 15 sccm and lower figure, labeled (b), is those of specimen B prepared at the NF_3 flow rate of 20 sccm. Deintercalation capacities of specimens A and B are about 130 and 290 mAh/g, respectively. The present results of charge and discharge measurements indicate that the crystallinity of carbon film at NF_3 of 20 sccm was higher than that of 15 sccm, which is in good agreement with the Raman spectroscopy results. The present flat films prepared by plasma CVD will be useful for the evaluation of interfacial properties between electrode and electrolyte.

3.4. Plasma etching of Si and SiO_2 surface using NF_3 [20,45]

The advantage of using NF_3 as an etchant over traditional carbon based etchants such as carbon tetrafluoride (CF_4) and hexafluoroethane (C_2F_6) includes high etching rate, high selectivity for nitride-over-oxide etching and single crystal silicon over thermally grown silicon oxide, and the production of only volatile reaction products, resulting in an etching without carbon based polymer or fluoride residues. Enhanced plasma or thermal cleaning of chemical vapor deposition (CVD) chambers is also a use of NF_3. Residual coating such as silicon are deposited on the internal surfaces of CVD chambers during deposition processes. A plasma using NF_3 can remove these deposits as volatile fluoride like SiF_4 at the process temperature, eliminating the need to remove the internal CVD chamber components to be cleaned by acid tank immersion. At present, large amounts of NF_3 is consumed as a dry etchant and a cleaning gas for the CVD chamber by the electronic industry in Japan.

Fig. 10 shows the cut-away views of etching Si using the NF_3 plasma. Upper figure, labeled (a), is a cut-way view of etching Si under conditions such as the NF_3 pressure of 70 Pa, gas flow rate of 400 sccm, and RF power of 50 W. In this case, the etching rate was 2.3 μm/min, but etching shape was isotropic. Lower figure, labeled (b), is under plasma conditions such as the NF_3 pressure of 70 Pa, gas flow rate of 100 sccm, and RF power of 50 W. Although the etching rate was 0.2 μm/min, etching shape was anisotropic.

Fig. 11 shows relationship between the etching rates of Si and SiO_2 and the ratio of NF_3 in the mixture gas of CF_4 and NF_3 under total pressure of 13 Pa. Although NF_3 was a good etchant for Si, the etching rate of SiO_2 using NF_3 plasma was smaller than that of Si and CF_4 was a better etchant for SiO_2. This is because oxygen component in SiO_2 may react with carbon component in CF_4 and be eliminated to form CO and/or CO_2.

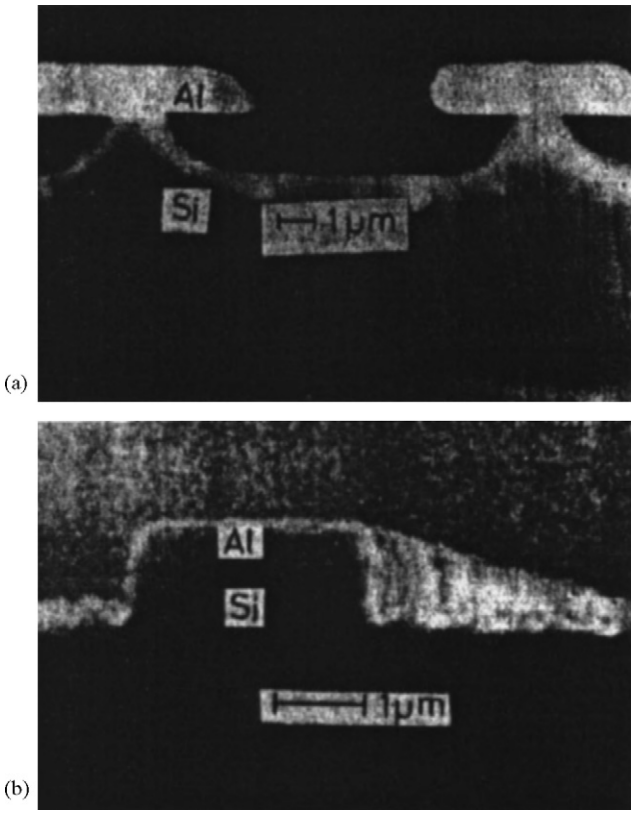

Fig. 10. Cut-away views of etching Si under various conditions: (a) NF_3 pressure = 70 Pa, gas flow rate of NF_3 = 400 sccm, RF power = 50 W, (b) NF_3 pressure = 70 Pa, gas flow rate of NF_3 = 100 sccm, RF power = 50 W.

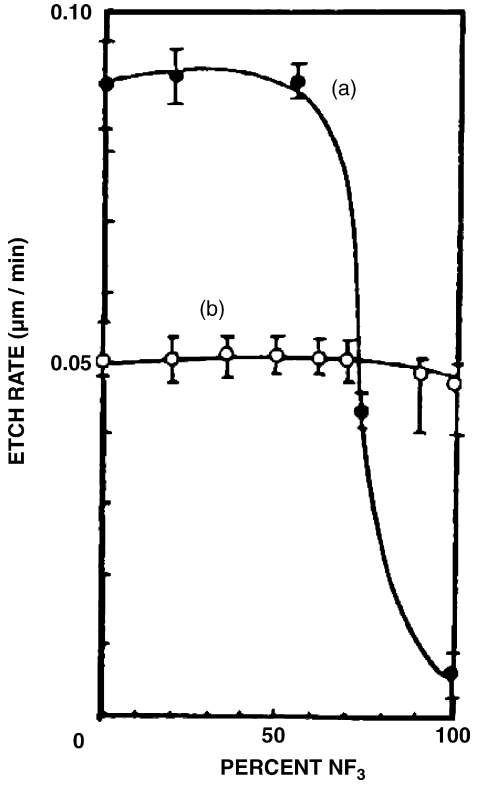

Fig. 11. Relationship between the etching rates of SiO_2 (a) and Si (b) and the flow rate ratio of NF_3 in mixture gas of CF_4 and NF_3. Total pressure of mixture gas = 13 Pa.

3.5. Plasma etching of SiC surface using NF_3 [46,47]

Silicon carbide (SiC) is a highly promising semiconductor material for use in high-temperature and high-power electronic-device applications such as automotive and aircraft engine monitoring microwave communications, thin-film transistor technology, light sensors, solar cells, and diagnostic medical imaging. This is because of the attractive properties of SiC, such as a wide band gap (2.3 eV) at 300 K, a high thermal conductivity (5 W/cm °C), its high breakdown electric field (3.0×10^6 V/cm), and high saturated electron-drift velocity (2.70×10^7 cm/s). However, poor machinability of SiC, which originates from its high mechanical strength and chemical stability, is a serious problem for use in these applications. Basically, all of the patterning steps during device processing must be carried out with dry etching owing to the chemical stability and inertness of SiC in conventional acid or base solutions at ambient temperature. In the present case, NF_3 is chosen as a fluorine radical ($F^\bullet$) source, because it efficiently decomposes to form free radicals and all possible reaction products are volatile, thus avoiding contamination or polymer formation in the CVD chamber.

Fig. 12 shows a variation of the etching rate of SiC and Si during reactive ion etching (RIE) at constant RF power of 100 W as a function of NF_3 pressure. The etching rate of SiC was much smaller than that of Si. The etching rate of SiC was large under NF_3 pressure ranging from 0.5 to 1 Pa and its value at NF_3 pressure of 1 Pa was 87 nm/min. It was decreased to reach a minimum value of 35 nm/min at NF_3 pressure of 3 Pa and then increased with increasing NF_3 pressure. A variation of the etching rate of SiC using NF_3/O_2 mixture gas plasma was similar to that using pure NF_3 plasma. From these results, it is found that relatively high etching rate of 87 nm/min can be obtained under the conditions such as RF power of 100–200 W and NF_3 pressure of 0.5–1 Pa. On the other hand, the etching rate of Si increased monotonously with increasing the NF_3 pressure.

Fig. 13 shows AFM images of SiC surface etched using NF_3 plasma. NF_3 pressure and RF power were kept constant at 1 Pa and 100 W, respectively. The surface of the specimen was

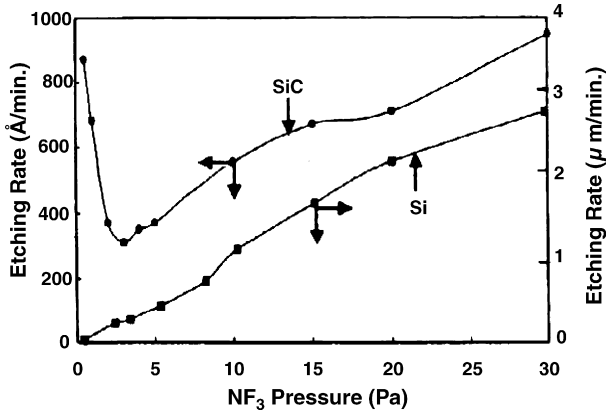

Fig. 12. A variation of the etching rate of SiC and Si during reactive ion etching (RIE) at constant RF power of 100 W as a function of NF_3 pressure.

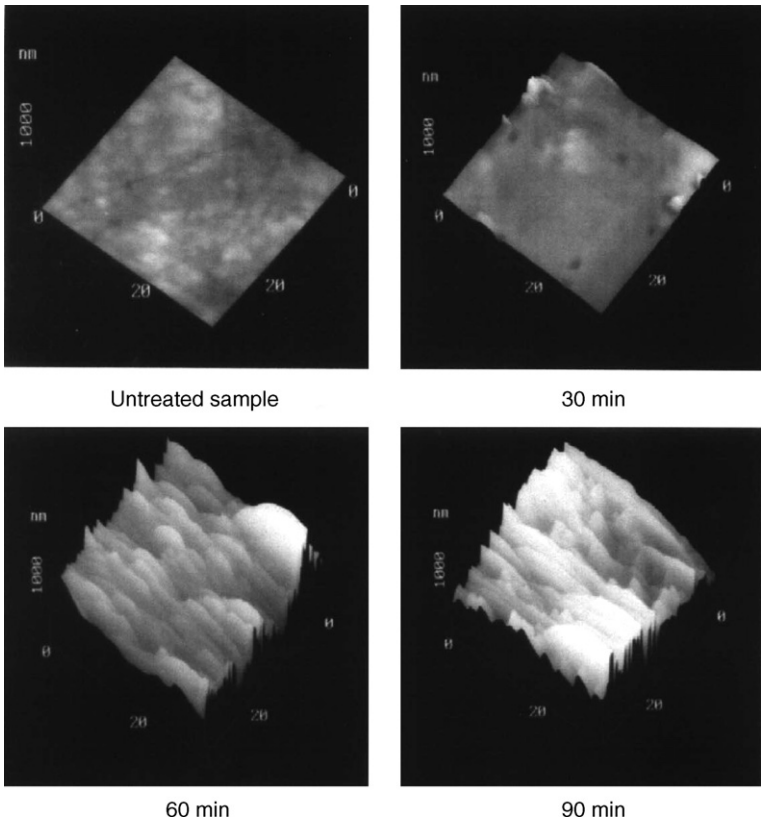

Fig. 13. AFM images of SiC surface etched using NF_3 plasama. NF_3 pressure = 1 Pa, RF power of 100 W.

smooth in the scale of nm within 30 min, whereas it became rougher over 60 min.

Fig. 14 shows SEM images of SiC surface etched at NF_3 pressure of 2 and 10 Pa. The SiC surface after etching using pure NF_3 plasma at NF_3 pressures lower than 2 Pa had a better smoothness, as shown in upper SEM image, whereas reactive ion etching (RIE) for SiC gave a rough surface consisting of many thorn-like residuals at NF_3 pressures higher than 3 Pa, as shown in lower SEM image. This was considered to be due to the preferential reaction of fluorine radical with the Si component of the SiC surface. The remaining carbon-rich part may act as a micro-mask to leave the carbon-rich thorns on the surface.

The SiC surface after etching using pure NF_3 plasma at NF_3 pressures lower than 2 Pa had a better smoothness, as shown in upper SEM image in Fig. 14. Although physical etching may mainly proceed at the NF_3 pressure of 2 Pa, little spike was observed on the SiC surface near the Al mask. Fig. 15a shows the TEM image of the cross-section of the spike formed on the SiC surface etched in the pure NF_3 plasma at the NF_3 pressure of 2 Pa. The 7 points on the surface and in the spike were analyzed by TEM and aluminum was detected only on the points 1 and 2. Fig. 15b also shows the C/Si ratio on each point on the surface and in the spike. This indicated that aluminum particle sputtered from the Al mask may be deposited on the carbon-rich region formed on the SiC surface and may act as a micro-mask to form many thorn-like spikes.

A SEM image of the rough surface, which had many thorn-like spikes, is also shown in Fig. 16. Although both positive ion such as N_2^+ and the activated radical species such as fluorine radical ($F^\bullet$) etch the SiC surface in the RIE reaction, chemical etching by activated radical species may mainly proceed during RIE under the NF_3 pressures higher than 3 Pa. The length of spike formed on the SiC surface increased with increasing etching time and increased gradually with increase of NF_3 pressure.

In the pure NF_3 plasma, positive ions such as F^{2+}, N^+, and N_2^+ and electric neutral species such as fluorine radical ($F^\bullet$) are present. As the intensity of species is proportional to its concentration, the relationship between the etching rate and the intensity of molecular nitrogen ion (N_2^+) or fluorine radical ($F^\bullet$) is shown in Fig. 17. Upper figure, labeled a, is that with respect to the N_2^+ intensity, and lower figure, labeled b, is with respect to the $F^\bullet$ intensity. The etching rate decreased with the increase of the intensities of N_2^+ and $F^\bullet$ to reach a minimum value at NF_3 pressure of 3 Pa and then increased with increasing them. This fact means that physical etching by N_2^+, i.e., ablation, may mainly proceed at NF_3 pressures lower than 3 Pa, because the chemical reaction of fluorine radical with the Si component on the SiC surface, i.e. chemical etching, may increase with the increase of the $F^\bullet$ concentration.

In order to attain a high etching rate and a smooth etched surface, oxygen was added to the NF_3 plasma [47]. Fig. 18 shows the optical emission spectrum in the NF_3/O_2 mixture gas plasma. It should be noted that oxygen radical ($O^\bullet$; line at 777 nm) is present in addition to species such as N_2^+ (line at 353.2 nm) and $F^\bullet$ (line at 703.7 nm) in the NF_3/O_2 mixture gas plasma. Fig. 19 shows a variation of intensities of N_2^+, $F^\bullet$ and

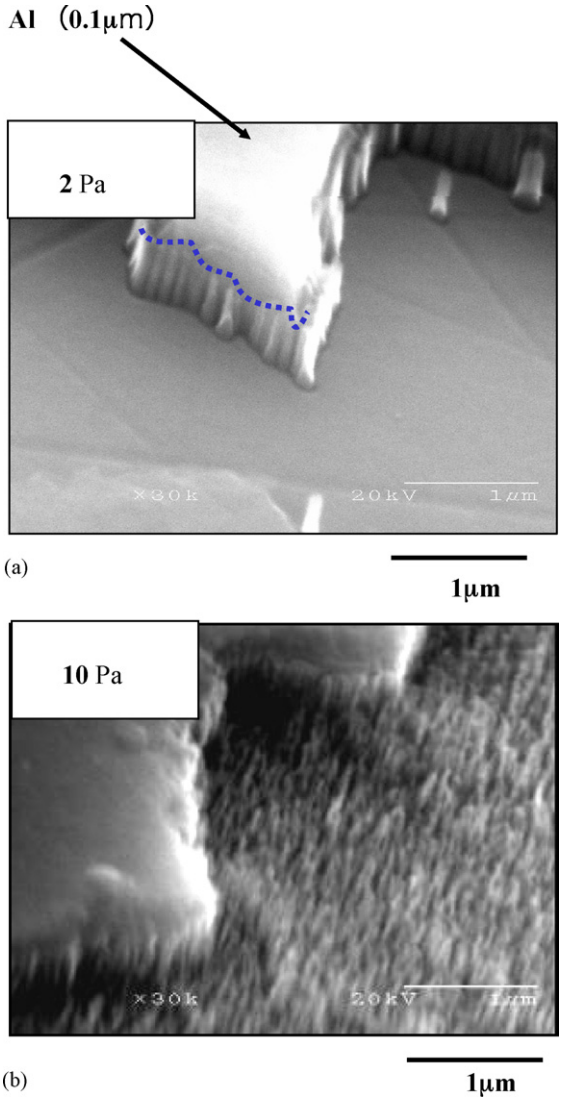

Fig. 14. SEM images of SiC surface etched at NF_3 pressure of 2 Pa (a) and 10 Pa (b).

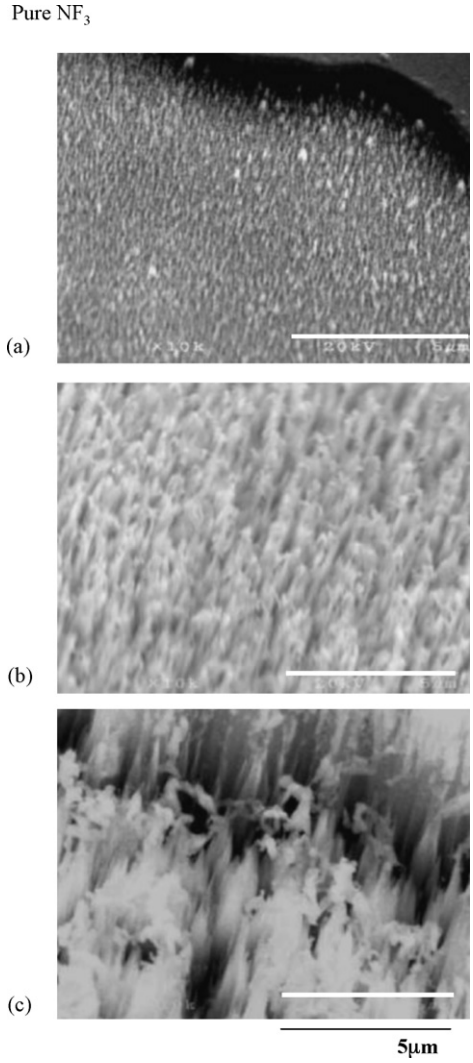

Fig. 16. SEM images of SiC surface etched in NF_3 plasma: effect of etching time on spike length. Etching time: (a) 10 min, (b) 30 min, and (c) 60 min.

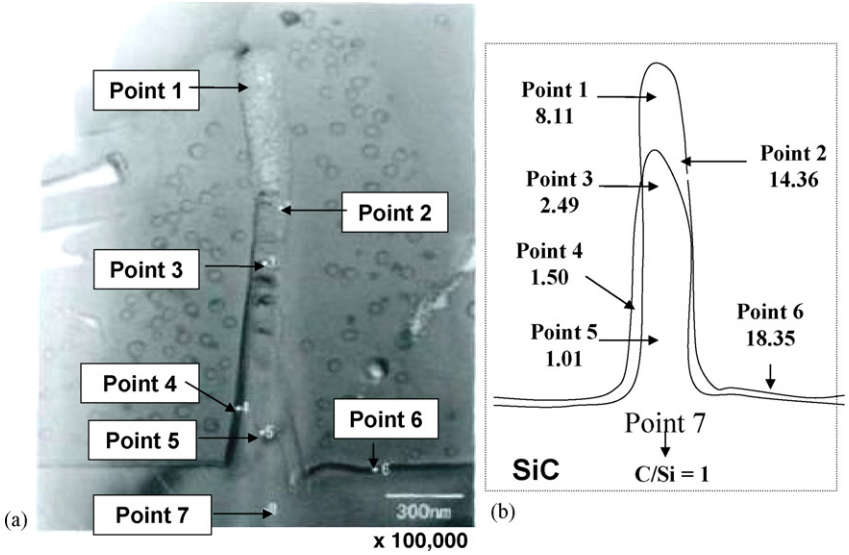

Fig. 15. TEM image of cross-section of spike formed on the SiC surface etched in pure NF_3 plasma at NF_3 pressure of 2 Pa. (a) TEM image of cross-section of spike, (b) ratio of C/Si on the seven points on the surface and in the spike.

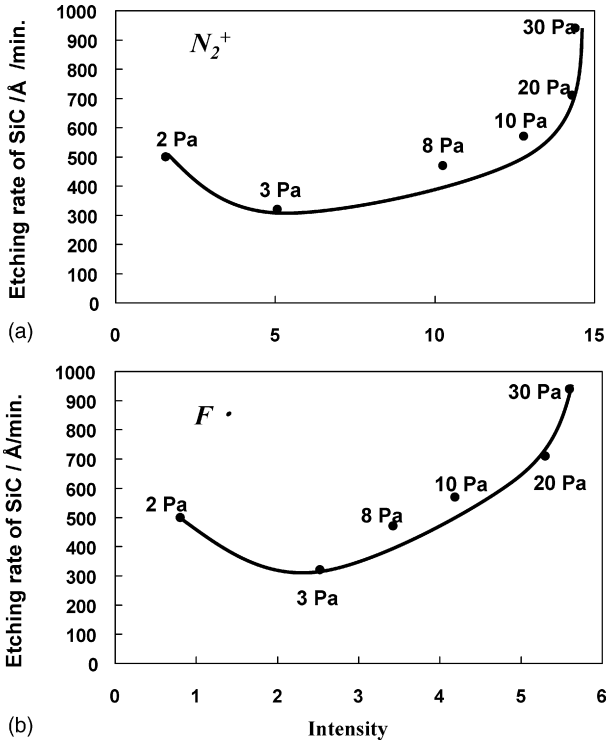

Fig. 17. Relationship between etching rate and intensities of nitrogen molecular cation (N_2^+) (a) and fluorine radical ($F^•$) (b).

$O^•$ in the NF_3/O_2 mixture gas plasma under conditions such as RF power of 100 W, total pressure of 10 Pa, and total flow rate of 10 sccm as a function of O_2 concentration. Intensities of N_2^+ and $F^•$ increased to reach their maximum value at the O_2 concentration of 10% and then decreased with increasing O_2 concentration. On the other hand, the intensity of $O^•$ increased and became almost constant at the O_2 concentration of 60%.

Fig. 20 shows a variation of the etching rate of SiC surface using the NF_3/O_2 mixture gas plasma under conditions such as RF power of 100 W, total pressure of 20 Pa, total flow rate of 10 sccm, and reaction time of 30 min as a function of O_2 concentration. The addition of 10% oxygen to the NF_3 plasma increased the etching rate to ca. 100 nm/min, but the further

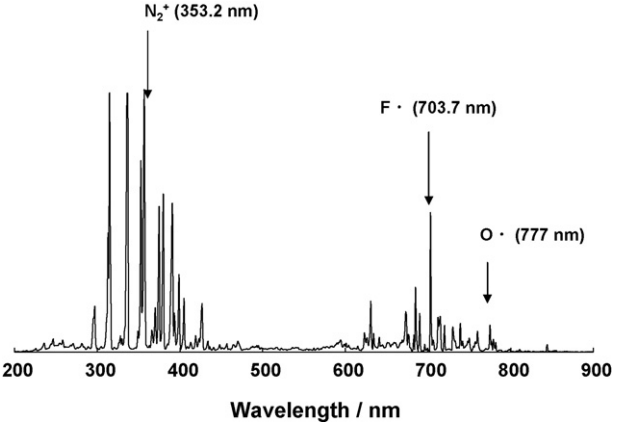

Fig. 18. Typical optical emission spectrum in NF_3/O_2 mixture gas plasma.

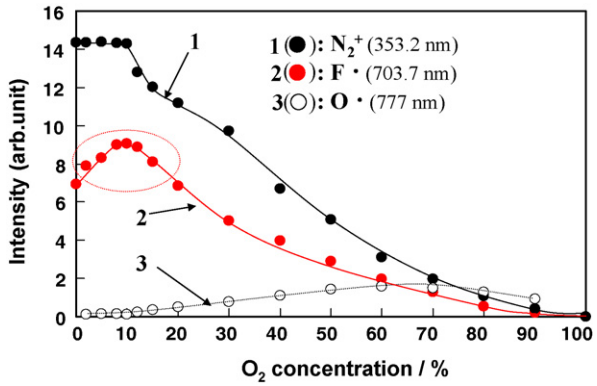

Fig. 19. A variation of intensities of nitrogen molecule cation (N_2^+), fluorine ($F^•$) and oxygen radical ($O^•$) in NF_3/O_2 mixture gas plasma as a function of O_2 concentration. RF power = 100 W, total pressure = 10 Pa, total flow rate = 10 sccm.

addition of oxygen decreased the etching rate, because of formation of SiO_2 on the SiC surface, which was resistant to etching using NF_3/O_2 mixture gas plasma. After that, the etching rate decreased monotonously with an increase in the O_2 concentration and then became negligible at O_2 concentrations higher than 50%.

Fig. 21 shows XPS spectra of C 1s, Si 2p, and O 1s levels on the SiC surface etched by NF_3/O_2 mixture gas spectra. C 1s spectra revealed that a peak at 285 eV assigned to carbon or graphite with covalent C–C bond appeared on the SiC surface. O 1s spectra also indicated that a peak at 103 eV assigned to SiO_2 appeared on the SiC surface. This means that SiO_2 is formed on the surface etched in the mixture gas plasma consisted of NF_3 (20%) and O_2 (80%) and so the etching of SiC may be prevented by SiO_2 formed on the SiC surface.

Fig. 22 shows SEM images of the SiC surface after etching for 60 min in the pure NF_3 plasma (a) and the NF_3/O_2 mixture gas plasma (b). The spike formed on the SiC surface after etching in the NF_3/O_2 mixture gas plasma was short compared with that in the pure NF_3 plasma. This means that addition of 10% O_2 to NF_3 is effective for suppression of the spike formation and its growth.

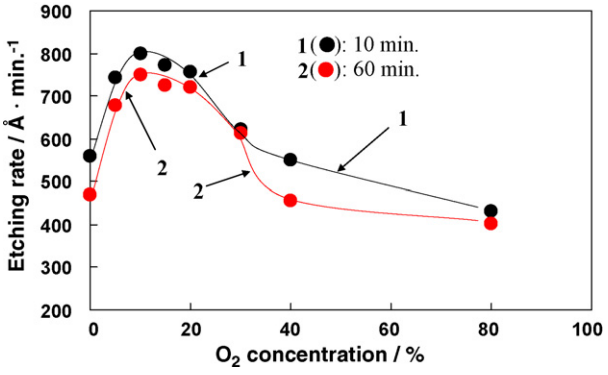

Fig. 20. A variation of etching rate of SiC surface using NF_3/O_2 mixture gas plasma as a function of O_2 concentration. RF power = 100 W, total pressure = 10 Pa, total flow rate = 10 sccm, etching time = 10 min (1) and 60 min (2).

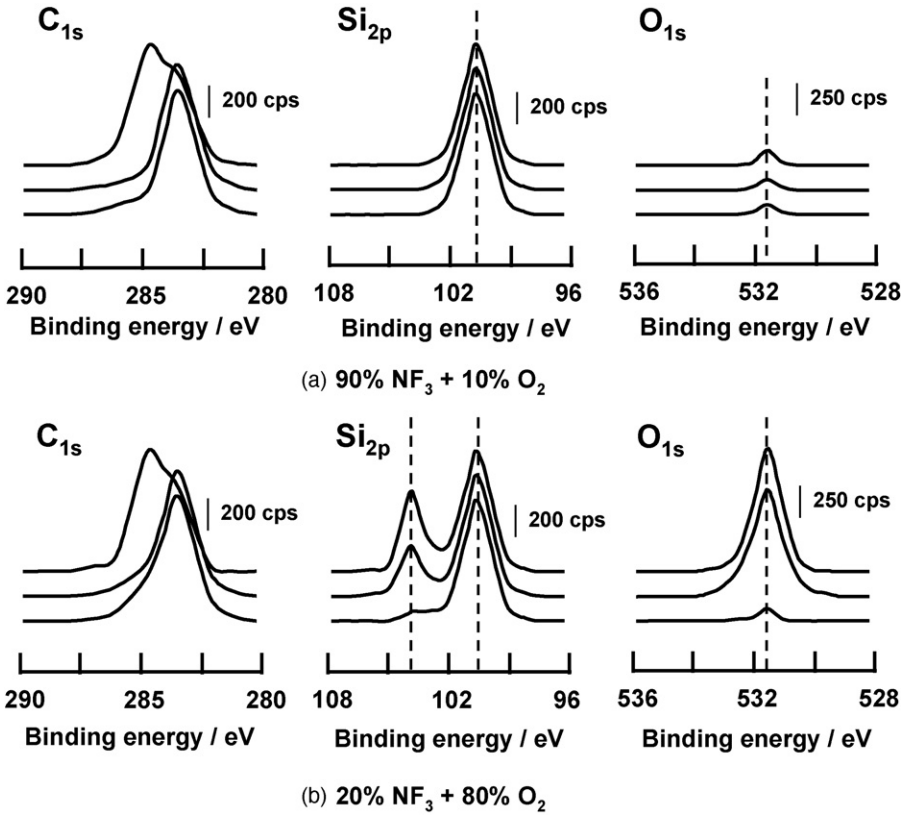

Fig. 21. XPS spectra of C 1s, Si 2p, and O 1s levels on SiC surface etched by NF_3/O_2 mixture gas plasma.

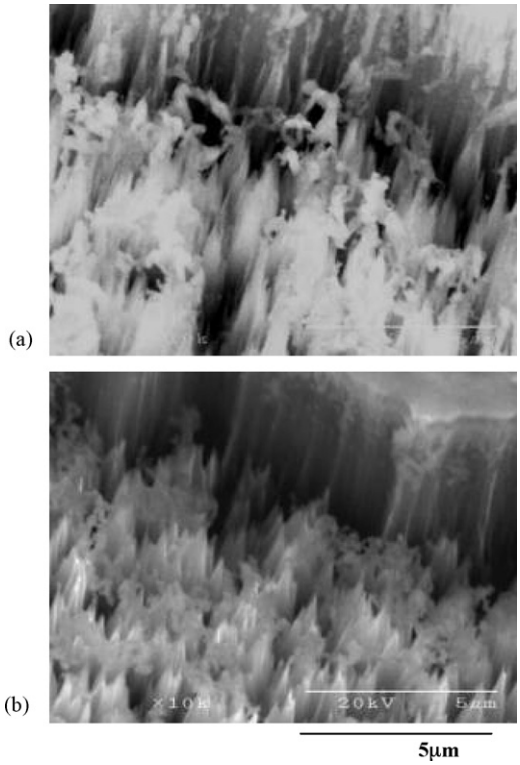

Fig. 22. SEM images of the SiC surface after etching for 60 min in the pure NF_3 plasma (a) and the NF_3/O_2 mixture gas plasma (b).

Consequently, it is considered that nitrogen molecular cation and fluorine radical are the main species for reactive ion etching of SiC using NF_3 plasma. A high etching rate and the surface smoothness of SiC were obtained simultaneously under plasma conditions such as the NF_3 pressure of 2 Pa, the input RF power of 100 W, and the NF_3 flow rate of 10 sccm. Although a high etching rate of SiC was obtained, many carbon-rich spikes were formed on the etched surface of SiC under the NF_3 pressures higher than 3 Pa. At the total pressure of 10 Pa, addition of 10% O_2 to NF_3 was effective for suppression of the spike formation and its growth.

Acknowledgements

This work was supported by a grant to Research Center for Advanced Science and Technology at Doshisha University from the Ministry of Education, Culture, Sports, Science and Technology, Japan and Scholarship contribution of Mitsui Chemicals, Incorporated.

References

[1] C.E. Colburn, Advances in Fluorine Chemistry, vol. 3, Butterworth, London, 1963, p. 52.
[2] H.C. Miller, F.D. Loomis, Encyclo. Chem. Tech., Fluorine Compound Inorganic (Nitrogen), vol. 11, third ed., 1966, p. 393.
[3] A. Tasaka, N. Watanabe, in: N. Watanabe (Ed.), Fusso to Kogyo II (Fluorine Chemistry and Industry Part II), Chemistry of Inorganic Fluorides—Fluoride Compounds of Nitrogen, Kagaku Kogyosha, 1984, pp. 1–34.

[4] K.O. McFadden, E. Tschuikow, J. Phys. Chem. 77 (1973) 1475–1478.
[5] G.L. Schott, L.S. Blair, J.D. Morgan Jr., J. Phys. Chem. 77 (1973) 2823–2830.
[6] E.A. Dorko, et al. J. Chem. Phys. 63 (1975) 3596–3601.
[7] P.J. Evans, E. Tschuikow-Roux, J. Chem. Phys. 65 (1976) 4202–4209.
[8] H.H. Rogers, Ind. Eng. Chem. 51 (1959) 309–310.
[9] C.J. Hoffman, R.G. Neville, Chem. Rev. 62 (1962) 1–18.
[10] M. Schmeiser, P. Sartori, Chem. Ing. Tech. 36 (1964) 9.
[11] O. Glemser, U. Bierman, J. Knaak, A. Haas, Chem. Ber. 98 (1965) 446–450.
[12] O. Glemser, U. Bierman, Chem. Ber. 100 (1967) 1184–1192.
[13] O. Glemser, J. Wegener, R. Mews, Chem. Ber. 100 (1967) 2474–2483.
[14] O. Glemser, U. Bierman, Chem. Ber. 100 (1967) 2484–2490.
[15] A. Tasaka, O. Glemser, Z. Anorg. Allg. Chem. 409 (1974) 163–170.
[16] Chem. Eng. News 43 (6) (1965) 47.
[17] J.L. Lyman, R.J. Jensen, Chem. Phys. Lett. 13 (1972) 421–424.
[18] J.L. Lyman, R.J. Jensen, J. Phys. Chem. 77 (1972) 883–888.
[19] D. Padrick, M.A. Gusinow, Chem. Phys. Lett. 24 (1974) 270–274.
[20] S. Nakayama, K. Tsuneto, A. Tasaka, T. Ohachi, D. Naito, I. Taniguchi, in: Proceedings of Second Symposium on Dry-process, Tokyo, October, (1980), pp. 115–122.
[21] K.M. Eisele, J. Electrochem. Soc. 128 (1981) 123–126.
[22] N.J. Ianno, K.E. Greenberg, J.T. Verdeyen, J. Electrochem. Soc. 128 (1981) 2174–2179.
[23] A. Kawamura, K. Tsuneto, T. Ohachi, T. Fujii, I. Taniguchi, in: Proceedings of Fourth Symposium on Dry-process, Tokyo, Octber, (1982), p. 39.
[24] Nikkei Microdevices (1985) 113.
[25] J.F. Tompkins, U.S. Patent 3,235,474 (1966).
[26] T. Tojo, J. Hiraiwa, N. Watanabe, Denki Kagaku (presently Electrochemistry) 66 (1998) 563–567.
[27] A. Tasaka, Curr. Top. Electrochem. 10 (2004) 1–36.
[28] T. Nakajima, T. Ogawa, N. Watanabe, J. Electrochem. Soc. 134 (1987) 8–11.
[29] N. Watanabe, Y. Chong, M. Aritsuka, M. Kanemaru, J. Mikami, in: Proceedings of the fourth Japan–China Bilateral Conference on Molten Salt Chemistry and Technology, Kyoto, Japan, (1992), pp. 111–114.
[30] O. Glemser, J. Schröder, J. Knaak, Chem. Ber. 99 (1966) 371–374.
[31] J. Massonne, Chem. Ing. Tech. 41 (1969) 695–742.
[32] A. Mimoto, Doctor Thesis, Doshisha University, 2006.
[33] A. Tasaka, H. Kobayashi, M. Negami, M. Hori, T. Osada, K. Nagasak, T. Ozaki, H. Nakayama, K. Katamura, J. Electrochem. Soc. 144 (1997) 192–197.
[34] A. Tasaka, Doctor Thesis, Kyoto University, 1970.
[35] A. Tasaka, N. Watanabe, Yoyuen (presently Molten Salts) 13 (1970) 152–173.
[36] A. Tasaka, Yoyuen (presently Molten Salts) 24 (1981) 195–226.
[37] A. Tasaka, T. Kawagoe, A. Takuwa, M. Yamanaka, T. Tojo, M. Aritsuka, J. Electrochem. Soc. 145 (1998) 1160–1164.
[38] M. Tramsek, B. Zemva, Acta Chim. Slov. 49 (2002) 209–220.
[39] A. Tasaka, A. Komura, Y. Uchimoto, M. Inaba, Z. Ogumi, J. Polym. Sci. A: Polym. Chem. 34 (1996) 193–198.
[40] T. Fukutsuka, T. Abe, M. Inabe, Z. Ogumi, N. Tsuji, A. Tasaka, Tanso (190) (1999) 252–256.
[41] F. Tuinstra, J.L. Koenig, J. Chem. Phys. 53 (1970) 1126–1130.
[42] G. Katagiri, Tanso (175) (1996) 304–313.
[43] D.S. Knight, W.B. White, J. Mater. Res. 4 (1989) 385–393.
[44] G. Katagiri, H. Ishida, A. Ishitani, Carbon 26 (1988) 565–571.
[45] K. Tsuneto, S. Nakayama, A. Kawamura, A. Tasaka, T. Ohachi, I. Taniguchi, Sci. Eng. Rev. Doshisha Univ. 24 (4) (1984) 252–261.
[46] A. Tasaka, K. Takahashi, K. Tanaka, K. Shimizu, K. Mori, S. Tada, W. Shimizu, T. Abe, M. Inaba, Z. Ogumi, T. Tojo, J. Vacuum. Sci. Technol. A 20 (4) (2002) 1254–1260.
[47] A. Tasaka, E. Watanabe, T. Kai, W. Shimizu, T. Kanatani, M. Inaba, T. Tojo, M. Tanaka, T. Abe, Z. Ogumi, J. Vac. Sci. Technol. A, submitted for publication.